Design, Fabrication and Testing of a Full-Scale Geopolymer Concrete Median Barrier

Milap Dhakal[1], Mir Al-Masud[1], Shaurav Alam[1], Carlos Montes[1], Kunal Kupwade-Patil[1], Erez Allouche[1] and Aziz Saber[2]

[1]Trenchless Technology Center, Louisiana Tech University, Ruston, LA 71270;
[2]Department of Civil Engineering, Louisiana Tech University, Ruston, LA 71270

KEYWORDS: geopolymer, fly ash, recycle, median barrier, finite element analysis

ABSTRACT

Geopolymer concrete presents a promising alternative to Portland-cement based concrete, offering high strength gain rate, enhanced corrosion resistance and lowered carbon footprints, while enabling the use of construction methods similar to those utilized in traditional OPC-based concrete applications.

This paper describes the application of fly ash based geopolymer concrete for the construction and testing of a full scale Jersey-type median barrier, a traffic divider structure commonly used by Departments of Transportation across the country. A constitutive finite element model was developed for the geopolymer concrete barrier to predict its structural response. In addition, an analytical solution was carried out using the yield-line failure theory. The geopolymer barrier was instrumented using 32 strain gages to monitor the strain during testing, and placed on a custom-built frame and tested to failure using a horizontally deployed, servo-controlled hydraulic actuator.

The measured response of the geopolymer barrier agreed well with finite element results as well as predictions obtained from the analytical analysis. The outcome of this study demonstrates that steel reinforced geopolymer concrete structures can be designed and analyzed using the same methods and theories used for reinforced concrete structures made using ordinary Portland cement. The results of the full-scale test also revealed that a geopolymer median barrier can be deployed safely in accordance with AASHTO LRFD.

1. Introduction

1.1 Background

The inherent characteristics of fly ash based geopolymer concrete (GPC) provides an alternative for traditional Ordinary Portland Cement (OPC) because of its ability to withstand external mechanical and environmental adversities. GPC was introduced in 1970s by French scientist Joseph Davidovits and refers to as a class of solid materials synthesized by the reaction of an aluminosilicate powder with an alkaline solution[1]. In recent years, a growing body of literature has become available regarding the chemical

and mechanical properties as well as durability characteristics of geopolymer concretes and grouts[2-4]. The growing interest in geopolymer binder technology over past two decades provides an indication of its wide-scale potential in the construction industry[5]. However, only limited studies are available regarding full scale applications of this emerging construction technology from a structural engineering prospective.

1.2 Current Research

Traffic median barriers are used by Departments of Transportation (DOTs) along highway systems to confine vehicular flow in prescribed pathways and to prevent errant vehicles from entering into the wrong lane or going out of the roadway. Like many other civil infrastructure elements, median barriers are subjected to environmental loads as well as mechanical loads. This is particularly true when such structures are deployed in coastal areas, where they are exposed to relatively high concentration of chlorine ions. Geopolymer concrete with appropriate chemical and physical properties[6-8] can be used as a alternative binder to the Portland cement in severe exposure conditions. Kupwade-Patil et al.[8, 9] demonstrated that carefully selected fly ash can be used to develop GPC with significantly higher resistance against the chloride induced corrosion and alkali-silica reaction in comparison to concrete derived from TYPE I cement. The use of locally available fly ash in order to construct a geopolymer median barrier provides a novel application of GPC binder technology, in a large scale application for the beneficent use of fly ash.

In addition to outstanding mechanical properties and durability characteristics, geopolymer technology is considered ‘green and eco-friendly’, as the use of fly ash as a binder offers a significantly lower CO_2 footprint compared with that associated with the production of Portland Cement[3, 6, 10] as well as a beneficial use of industrial byproducts, energy conservation, and conservation of virgin materials.

The design and detail specifications for median barriers are provided by the American association of state highway and transportation officials (AASHTO). These specifications have been periodically modified so as to incorporate changes in the vehicular type and loading mandated on federal and state highways. By 2009, AASHTO published its revised Load Resistance Factor Design (LRFD) which is a design guide for bridges and their fixtures[11]. This update superseded the NCHRP Report 350[12], which had been the accepted method for safety hardware device testing and acceptance since 1993. The LRFD (2009) incorporates the various vehicular loads and crash conditions to assure roadside safety performance of traffic barriers.

To ascertain the compatibility of the geopolymer bridge barrier, it was imperative to design it according to the prevailing code of practice i.e. AASHTO LRFD and AASHTO MASH. Fabrication also followed current construction practices used in the production of OPC median barriers.

2 Materials and Methods

New Jersey (NJ) type median barrier design was chosen for this study. A working drawing with detailed layout was obtained from Waskey Bridges Inc., of Baton Rouge, LA. This layout has been used by Waskey for their OPC based barriers. A simplified drawing highlighting the main features of the NJ median barrier is shown in Figure 1.

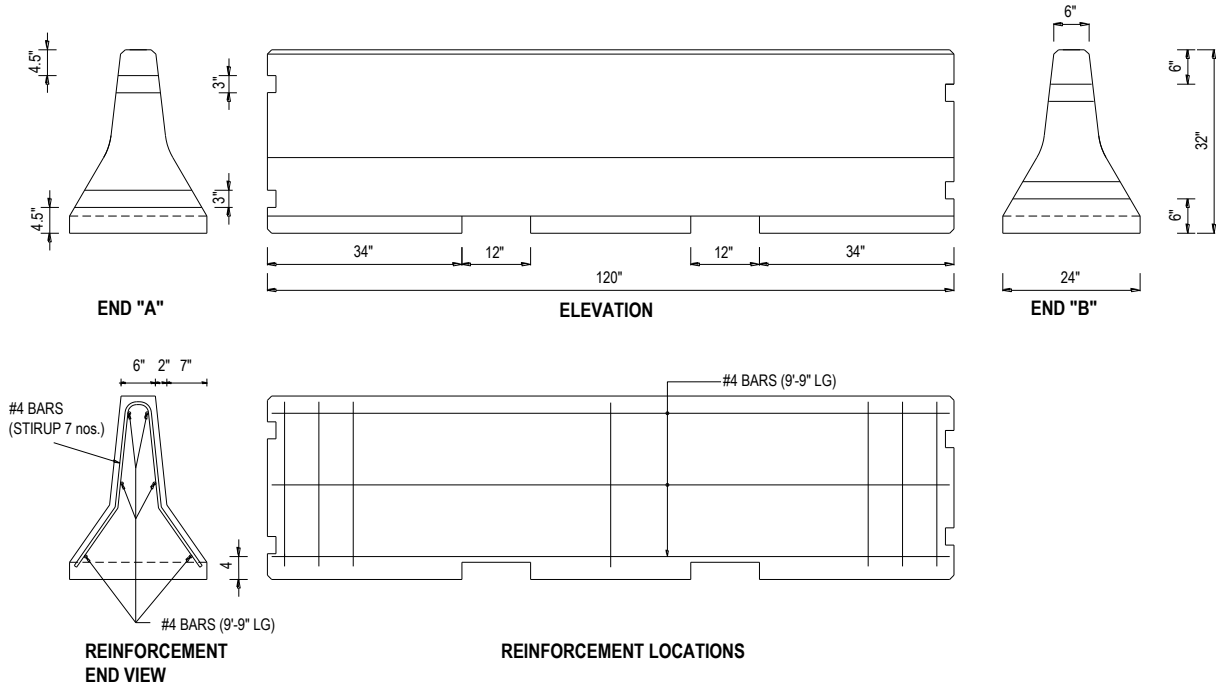

Figure 1. Schematic diagram of the median barrier (After Waskey Bridges Inc., *All dimensions are in inches unless specified otherwise)*

2.1 Theoretical Work

Yield line analysis utilizes the capacity of the reinforcing steel, and hence provides an estimation of the ultimate load a reinforced concrete section can carry prior to failure. Calculations were carried out on the basis of the details given in the Figure 1. The analytical evaluation of the NJ bridge barrier was carried out as per AASTHO LRFD specifications. The LRFD specification uses the simplified yield line analysis method which was proposed by T.J. Hirsch[13].

Sectional capacity of the precast concrete barrier is estimated based on the formation of yield lines at limit state. The yield-line method is a procedure where the structure is assumed to behave inelastically and exhibits adequate ductility to sustain the applied load until the slab reaches a plastic collapse state. This assumption is realistic because the reinforcement proportionality required by AASHTO results in an under-reinforced ductile system. The slab is assumed to collapse under the application of its ultimate load through a system of plastic hinges called yield lines. The yield lines form a pattern in the slab, creating a failure mechanism. The ultimate load can be determined using the energy (Virtual Work) approach. The energy approach is an upper-bound approach,

which means that the ultimate load established with this method is either equal to or greater than the actual load. The fundamentals and the primary assumptions behind the yield line theory are as follow[14, 15]:

- In the mechanism, the bending moment per unit length along all yield lines is constant and equal to the moment capacity of the section.
- The slab parts (area between yield lines) rotate as rigid bodies along the supported edges.
- The elastic deformations are considered small relative to the deformation occurring in the yield lines.
- The yield lines on the sides of two adjacent slab parts pass through the point of intersection of their axes of rotation.

The assumed yield line pattern caused by a vehicular collision that produces a force, F_t, is distributed over a length L_t and that the yield line pattern is consistent with the geometry and boundary conditions of the structural element under consideration. The analytical solution is obtained by equating the external work due to the applied loads to the internal work delivered by the resisting plastic moments along the yield lines. The applied load determined by this method is either equal to or greater than the actual load, which implies that the method is generally non-conservative.

External Virtual Work

The original and deformed positions of the top of the wall are shown in Figure 2.

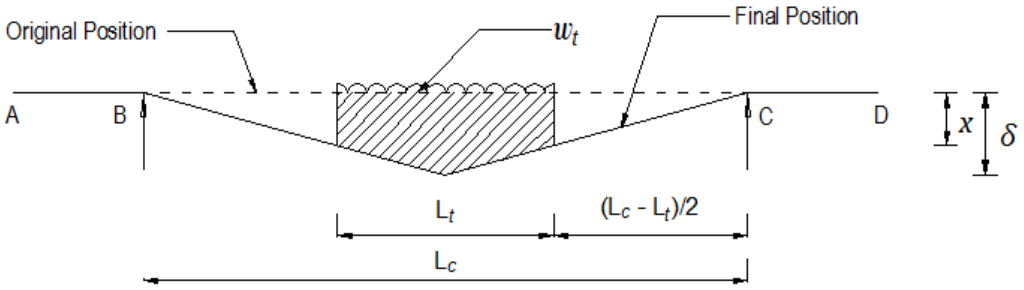

Figure 2. Original and deformed positions of the barrier wall[16]

The shaded area represents the integral of the deformations through which the uniformly distributed load $w_t = F_t/L_t$ acts. For a virtual displacement, δ , the displacement x is:

$$x = \frac{L_c - L_t}{L_c}\delta \tag{1}$$

Therefore, $$Area = \frac{L_t}{L_c}\delta\left(L_c - \frac{L_t}{2}\right) \tag{2}$$

Thus, the external work done by the load w_t can be expressed as shown in Equation(3) and Equation (4).

$$W_E = w_t \times Area = \frac{L_t}{L_c}\delta\left(L_c - \frac{L_t}{2}\right) \quad (3)$$

$$W_E = F_t\,\delta\,\frac{2L_c - L_t}{2L_c} \quad (4)$$

Internal Virtual Work

The internal virtual work along the yield lines is the sum of the products of the yield moment and the rotation caused by the corresponding moments. For simplicity of the analysis, different yield mechanisms are separately analyzed. Failure of the barrier is assumed to take place by flexure along a horizontal axis (M_c) and a vertical axis (M_b and M_w).

Unlike the original proposed yield line mechanism of Hirsh et al.[13], in the case of the median concrete barrier considered in this study, which is not fixed at the base (Gravity Standing), the cantilever effect on the barrier wall can be ignored i.e., $M_c = 0$. Hence, the bending moment causing the barrier to yield is only along its vertical axis, and in the analysis of the ultimate transverse load the internal work done is limited to the moment acting along the vertical axis. The plastic mechanism of the barrier wall is given in Figure 3. We assume the M_w to be constant about the vertical axis, thus the expression for the internal work done $U_{w,}$ can be written as in Equation (6).

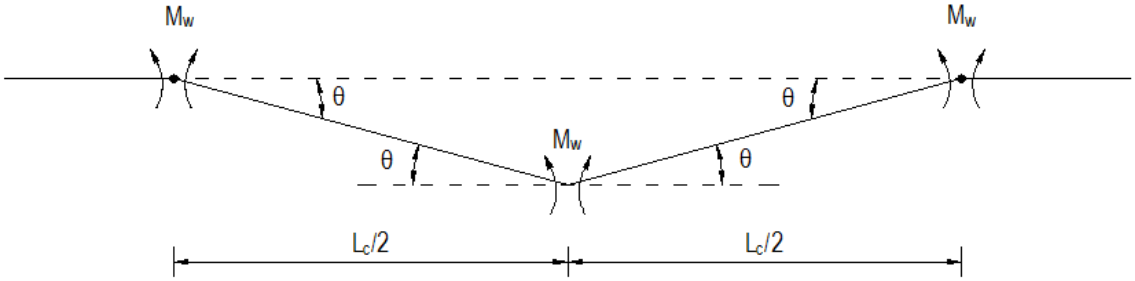

Figure 3. Plastic hinge mechanism for top beam as suggested by Calloway[16]

Let, θ be the angle of rotation due to the flexure, $\theta \approx \tan\theta = \frac{2\delta}{L_c}$ (5)

If we assume that the positive and negative bending resistance Mw about the vertical axis are equal, and we designate the projection on the horizontal plane of the rotation about the inclined yield line to be δ, the internal work U_w done by the wall moment M_w can be expressed as:

$$U_w = 4 \times M_w \times \theta = 8 M_w \frac{\delta}{L_c} \quad (6)$$

Next, we equate the internal virtual work done to the external virtual work done in the system and solve for F_t,

$$F_t \delta \frac{2L_c - L_t}{2L_c} = 8 M_w \frac{\delta}{L_c} \quad (7)$$

$$\text{Or, } F_t = \frac{8 M_w}{(L_c - \frac{L_t}{2})} \quad (8)$$

2.2 Finite Element Analysis

A constitutive finite element (FE) model for the median barrier was developed in ANSYS, commercially available FE software, and was validated by comparing the numerical prediction with the analytical solution. The finite elements of the model were created using the discrete approach, i.e. modeling with direct creation of the nodes. These nodes were used to create the corresponding GPC and re-bar elements (see Figure 4). Table 1 illustrates the selected element types along with their respective constitutive characteristic features.

Table 1. Element Selection for the FE modeling

Material	Element	Features	Material Properties
Reinforcing Steel	LINK8	Uniaxial tension-compression, plasticity, creep, swelling, stress stiffening, and large deflections	f_y=60,000 psi, X-area=0.2in^2, E=29x10^6, Poisson's ratio=0.3
Geopolymer Concrete	SOLID65	Crack analysis, nonlinear material property	f'_c=5,200 psi, E=2.39x10^6 psi, Density=140 pcf, Poisson's ratio=0.2

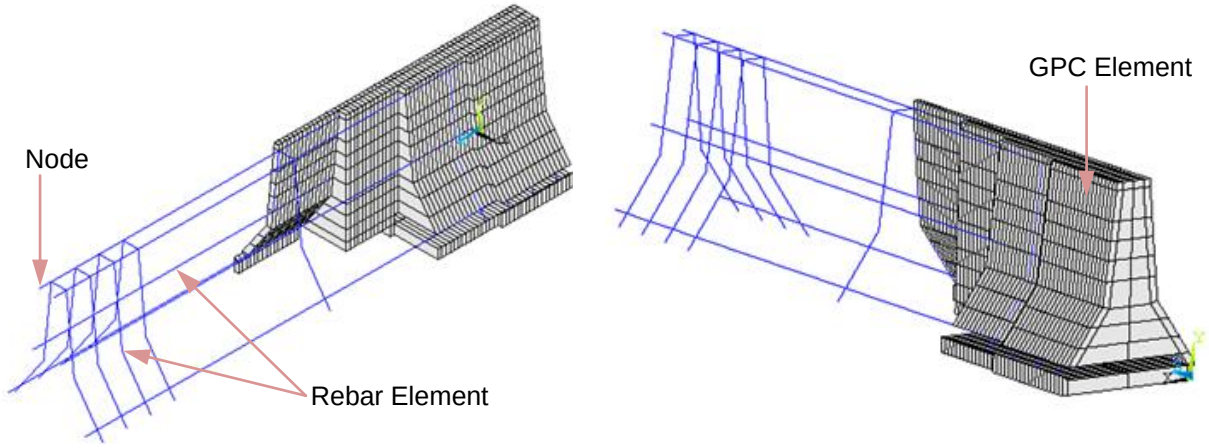

Figure 4. Simulation of concrete and steel elements

The properties of the materials were obtained from laboratory testing following relevant ASTM standards[17, 18]. The key properties of the materials obtained from the GPC and steel testing are summarized in Table 1. The strain-stress curves inputted into the FE model are given in Figure 5.

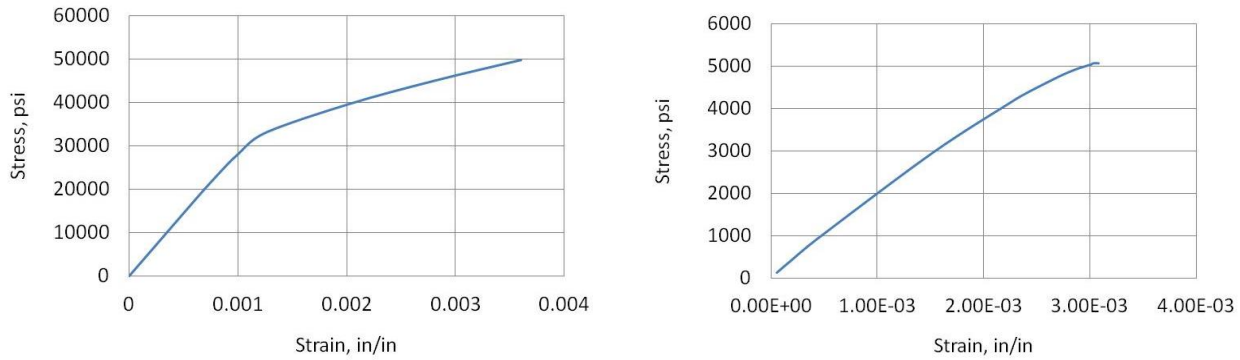

Figure 5. Stress-strain curves used for reinforcement steel (Left) and GPC (Right)

To approximate the cracking load for the GPC barrier, cracking properties were also incorporated in the constitutive model (see Table 2). In addition, appropriate boundary conditions representing the support conditions of the experimental setup were assigned.

Table 2. Cracking properties of the geopolymer concrete

Properties	**Value**
Open Shear Transfer Coefficient	0.3
Closed Shear Transfer Coefficient	0.7
Uniaxial Cracking Stress	650 psi
Tensile Crack Factor	1

2.3 Fabrication of Full Scale Jersey-Type Traffic Barrier

Locally available river sand with fineness modulus (FM) of 2.0, and alluvial gravel with nominal size 3/8" were selected as the aggregates for the GPC mix design. Fly ash generated by Dolet Hills thermal power plant, Mansfield, LA was used as the fly ash precursor for the derivation of the geopolymeric binder. The chemical composition of the fly is given in Table 3, and was found to be in agreement with ASTM class-F specifications (low CaO)[19].

Table 3. Chemical Composition of the selected fly ash

Compound	SiO_2	Al_2O_3	MgO	Na_2O	SO_3	TiO_2	MnO_2	BaO	Fe_2O_3	CaO	K_2O	SrO
%Composition	56.04	20.93	1.45	0.59	0.23	1.84	0.21	0.15	11.29	5.67	1.39	0.13

In addition, particle size analysis was conducted on the FA, which showed that 90% of the fly ash sample was finer than 45μm. Freshly prepared, highly concentrated NaOH solution and commercially available Na_2SiO_3 (SiO_2:Na_2O ratio of 3.22 and density 11.6 lb/gal) were used to activate the fly ash so as to achieve the polymerization reaction. Trial mixing was conducted for the optimized mix design to confirm compliance of the compressive strength with the requirements of AASHTO for bridge barriers. Some of the key parameters of the optimized mix design are illustrated in Table 4.

Table 4. Mix design parameters

Parameters	Levels
Fine Aggregate	Sand
Coarse Aggregate	Pea-Gravel
Binder	Fly Ash
Fly Ash : Aggregate	1:4
Activator : Fly Ash	0.41

The fabricated rebar cage was placed in a custom made wooden formwork. The steel cage was instrumented with 18 strain gages, so as to capture the strains developed in the steel rebars during the loading of the barrier. Details of the strain gage locations in the rebar cage are shown in Figure 6. Next, the geopolymer concrete was mixed and placed in the formwork in a similar fashion to that used for OPC mixes. The GPC median barrier was left for the ambient temperature (~80^{o}F) curing for 14 days.

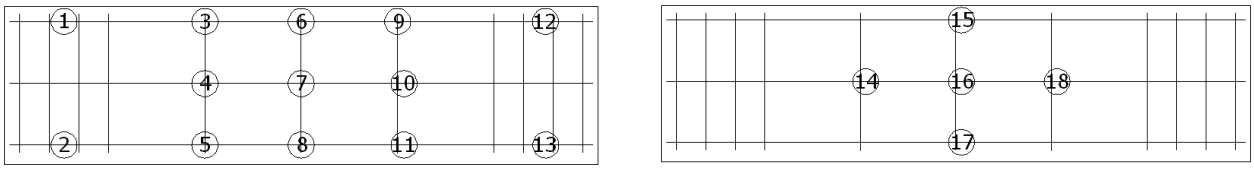

Tensile Side Strain Gage Location

Compressive Side Strain Gage Location

Figure 6. Strain Gage Schedule on the Rebars

2.4 Full Scale Testing

The wooden formwork was stripped off and the cured GPC median barrier was transported to the TTC's testing facility. The barrier was placed on a custom made steel frames bolted to the strong floor, mimicking on-site loading conditions. Horizontal load was applied using a 330 kip actuator (see Figure 7(Left)). A steel beam (6"×6"×36") was attached to the head of actuator ram, to ensure that the external load is applied in a uniform manner to the surface of the barrier.

The median barrier was tested in a 'Load Control' fashion. Loading was applied in increments of 2 Kips, and the barrier was thoroughly checked for cracking following each load increment. Cracks were marked and designated with sequential labels as shown in Figure 7(Right).

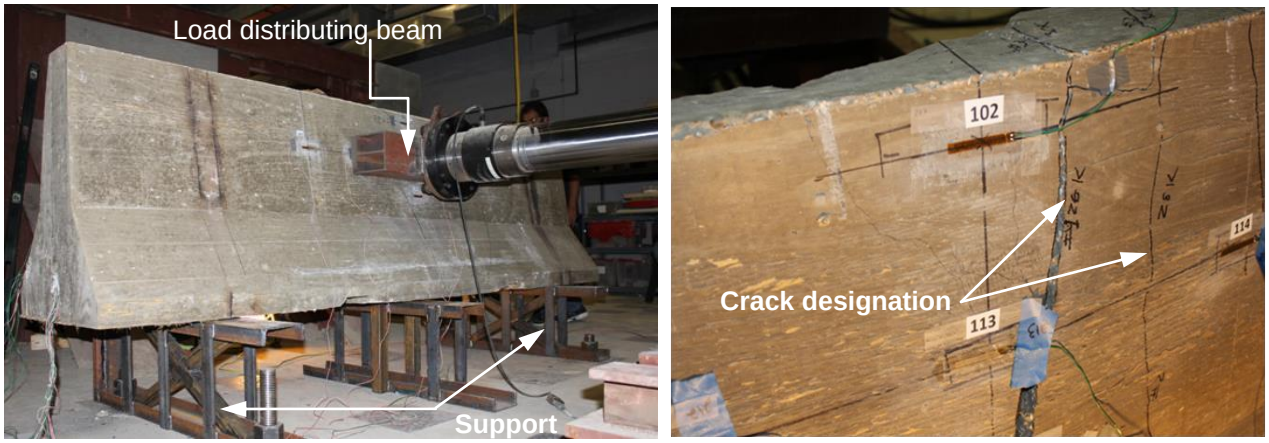

Figure 7. Barrier placed on bolted supports in front of the actuator (Left) and Crack designation and markings (Right).

A simplified free body diagram of the laboratory testing of the median barrier is shown in Figure 8. R_B and R_E are the reactions at the two supports and w is the uniformly distributed load acting on the barrier.

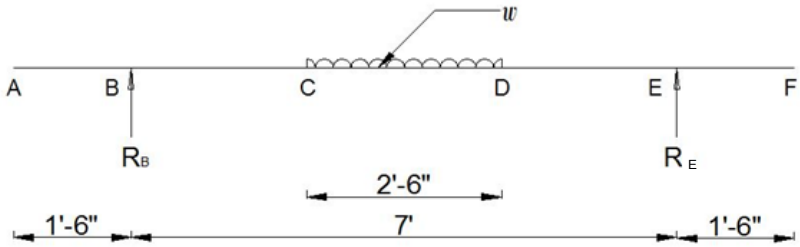

Figure 8. Free body diagram of the loading condition

Fourteen strain gages, each 2” long, seven on tensile side and seven on compressive side, were attached to the concrete surface in order to record strain on the outermost fiber of the GPC barrier (see Figure 9 for placement plan). Readings from strain gages were taken in a continuous fashion during the entire test.

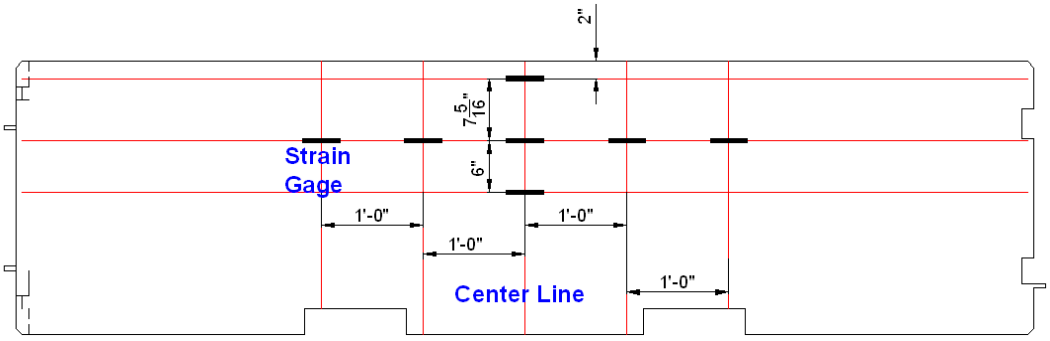

Figure 9. Location of strain gages placed on the surface of the GPC barrier

3 Results and Discussions

3.1 Validation of FE model

The finite element model was validated by comparing its predictions with those obtained from a classical analytical solution. The flexural relation given in Equation (9) was used in the analysis.

$$\sigma = \frac{M}{I} \times Z \tag{9}$$

Where, maximum bending moment (*M*) and moment of inertia (*I*) were calculated using the free body diagram and details of the transverse section of the traffic barrier (refer Figure 8 and Figure 10). Loads in the FE model were kept low, so as to maintain the material in a linear elastic state. The accuracy of FE model was evaluated by comparing the maximum bending stress obtained from the FE analysis with the analytical solution. The comparison is shown in Table 5.

Table 5. Comparative Study of validity of FE results against analytical solution

Total Applied Load, lb	UDL (*w*), lb/in	Bending Stress, (psi)		% Error
		Analytical Calculation (σ=0.455w), lb/in^2	FE Model (σ), lb/in^2	
100	3.33	1.52	1.65	8.55
500	16.67	7.58	8.27	9.10
800	26.67	12.13	13.23	9.07

3.2 Determination of Ultimate Failure Load

To compute the ultimate load that the structure can sustain prior to failure, a yield line analysis was carried out based on the sectional details of the barrier. When the vehicle load is applied to the barrier, the barrier bends about its vertical axis. The section resisting this bending mechanism is hence the transverse section of the barrier. The geometrical parameters used for estimation of the moment of resistance (M_oR) are shown in Figure 10.

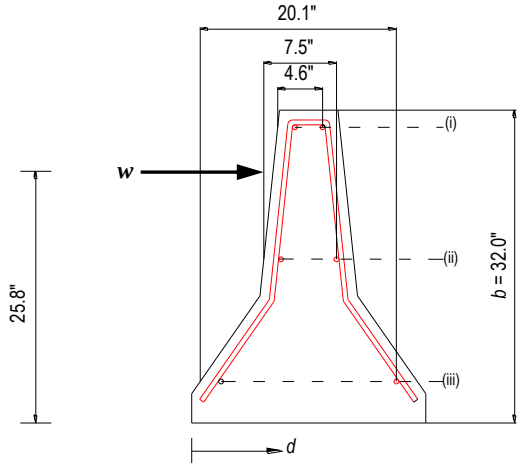

Figure 10. Sectional view showing the variation of effective depth for different rebars

$$M_w = A_s f_y (d - a/2) \quad (10)$$

Where,

A_s = area of reinforcing steel resisting the flexural tension = 3×0.2 = 0.6 in^2,
f_y = yield strength of the steel reinforcement = 60,000 lb/in^2,
f'_c= characteristic compressive strength of GPC = 5,200 lb/in^2,
d = effective depth of the beam (varying according to the location of re-bars)
= 4.6", 7.5" and, 20.1" respectively at layer i, ii and iii,

$$a = \frac{A_s f_y}{0.85 f'_c b} \quad (11)$$

The computation of the total M_oR corresponding to the bending about the vertical axis of the barrier are tabulated in Table 6.

Table 6. Computation of M_w

Bar Layer	D, in	*d*, in	(*d*-*a*/2), in	M_n, lb-in	M_n, Kip-ft	ΣM_n, Kip-ft
i.	6.40	4.60	4.37	52465.20	4.37	
ii.	9.20	7.50	7.27	87265.20	7.27	31.52
iii.	22.30	20.10	19.87	238465.20	19.87	

With the barrrier being simply supported, the plastic hinges are expected to form at the supports. Hence, substituting L_c = 7', L_t = 1'- 6", and the calculated value of ΣM_n = 31.52 Kip-ft into Equation (8), the ultimate load bearing capacity of traffic barrier (F_t) was computed to be 45.85 Kip.

3.3 Experimental Investigation and Comparison of Results

Crack analysis of the barrier's FE model predicted the first crack to appear at a load of 30 Kip, whereas the initiation of cracking during the test was observed to occur at 26 Kip. This suggests a close agreement with the FE approximation. The load displacement characteristics of the GPC barrier are shown in Figure 11. As the load reached 30 Kip, the first crack fully propagated on the tensile face of the barrier, along with the development of a second crack. When the applied load reached 32 Kip, a shear crack was observed at the right support while the crack at the central tensile zone (first crack) developed further. The flexural load was completely transferred to the rebar at 41 Kip, when the concrete fully cracked, which was accompanied with loud sound. The steel was visible at this point and the load dropped to 22 Kip. As the load further increased, the rebar failed when the load reached 26 Kip. This marked the end of the test.

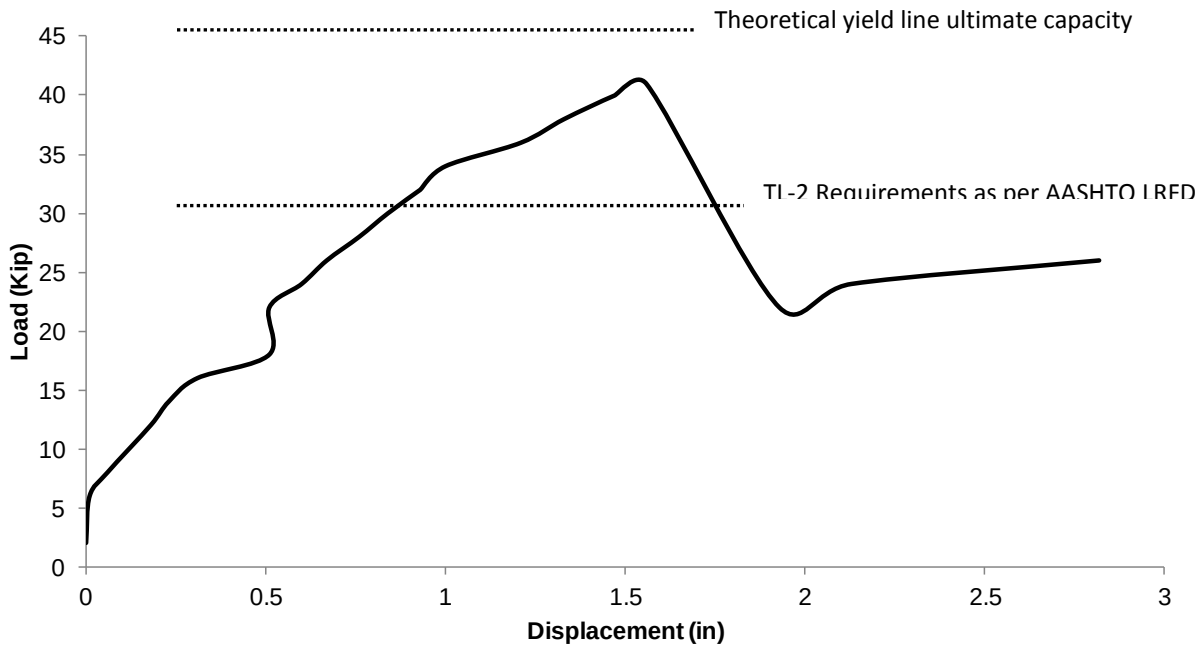

Figure 11. Experimental load displacement characteristics

The comparison of the bending stresses obtained from the analytical and numerical solutions with the experimentally measured values are shown in Figure 12. It was found that overall, the experimentally measured results were in close agreement with the values predicted by the numerical and analytical solutions.

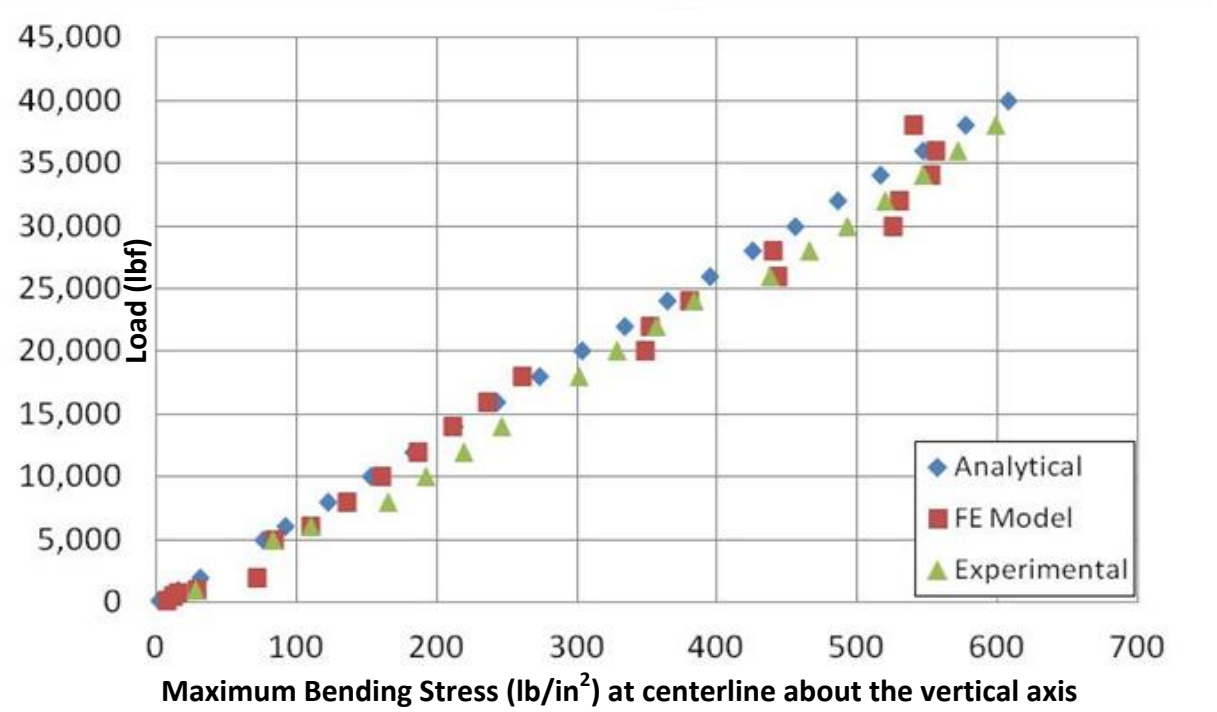

Figure 12. Comparison of obtained bending stress

The ultimate load (F_t = 41 Kip) obtained from the experiment was checked for the test level (TL) compliance recommendation of AASHTO LRFD (see Table 7). Since, the total height of the constructed median barrier (*H)* was 32" with height of load (H_e) = 25.8" which is greater than minimum allowable values (27" and 20" respectively), the median barrier can be considered to comply with TL-2 requirements of the AASHTO LRFD.

Table 7. Design forces for traffic railings (Table A13.2-1)[11] and comparison with studied barrier

Design Forces and Designations	Railing Test Levels				GPC Barrier
	TL-1	TL-2	TL-3	TL-4	
F_t Transverse (Kips)	13.5	27.0	54.0	54.0	41.0
L_t (ft)	4.0	4.0	4.0	3.5	2.5
Minimum *H* Height of Rail (in)	27.0	27.0	27.0	32.0	32
H_e (min) (in)	18.0	20.0	24.0	32.0	25.8

4 Conclusions

A full scale Jersey type barrier was constructed using geopolymer concrete following the applicable standards of AASHTO LRFD and tested to failure. The testing revealed performance with compliance equivalent to Railing Test Level TL-2 as per AASHTO LRFD. Thus, the barrier could potentially be accepted for work zones in most of the local and collector roads with favorable site conditions (roadways where small number of heavy vehicles is expected and posted speeds are reduced[11]).

The study demonstrates that GPC, like the OPC concrete can be batched, mixed, transported and placed to cast structural elements, using traditional construction methods and equipment. Standard material testing techniques used for OPC concrete were shown to be acceptable of measuring the mechanical properties of GPC. The close agreement of the experimentally measured values with both, FE and yield line analysis, implies that the use of structural analysis and design approaches deployed for steel reinforced Portland cement concrete can be adopted for the steel reinforced geopolymer concrete structures.

Acknowledgement

The authors would like to acknowledge the financial support provided by Louisiana Transportation Research Center via Grant LTRC 11-12 TIRE. The in-kind support provided by Mr. Sims Regard and Waskey Bridges Inc. of Baton Rouge is also acknowledged.

REFERENCES

1. Davidovits, J., *Geopolymer Chemistry and Applications*2011: Institut Géopolymère.
2. Provis, J.L. and Van Deventer, J.S.J., *Geopolymers: Structure, Processing, Properties and Industrial Applications*2009: Woodhead Publishing Limited.
3. Diaz-Loya, E.I., Allouche, E.N. and Vaidya, S., *Mechanical properties of fly-ash-based geopolymer concrete.* ACI Materials Journal, 2011. 108(3): p. 300-306.
4. Montes, C. and Allouche, E., *Influence of Activator solution formation on fresh and hardened properties of low-calcium fly ash geopolymer concrete.* Coal Combustion and Gasification Products Journal, 2012. 4: p. 1-9.
5. Duxson, P., Fernández-Jiménez, A., Provis, J., Lukey, G., Palomo, A. and van Deventer, J., *Geopolymer technology: the current state of the art.* Journal of Materials Science, 2007. 42(9): p. 2917-2933.
6. Diaz, E.I., Allouche, E.N. and Eklund, S., *Factors affecting the suitability of fly ash as source material for geopolymers.* Fuel, 2010. 89(5): p. 992-996.
7. Kupwade-Patil, K. and Allouche, E., *Examination of Chloride Induced Corrosion in Reinforced Geopolymer Concretes.* Journal of Materials in Civil Engineering. DOI:10.1061/(ASCE)MT.1943-5533.0000672.
8. Kupwade-Patil, K., Allouche, E., Vaidya, S. and Diaz-Loya, E., *Corrosion analysis of reinforced geopolymer concretes*, in *Concrete Solutions 2011*2011, CRC Press.
9. Kupwade-Patil, K. and Allouche, E., *Impact of Alkali Silica Reaction on Fly Ash-Based Geopolymer Concrete.* Journal of Materials in Civil Engineering, 2013. 25(1): p. 131-139.
10. Friedlingstein, P., Houghton, R.A., et al., *Update on CO2 emissions.* Nature Geoscience, 2010. 3(12): p. 811-812.
11. AASHTO, *AASHTO LRFD Bridge Design Specifications*2012, Washington: AASHTO.
12. H. E. Ross, J., D. L. Sicking, R. A. Zimmer, J. D. Michie, *Recommended Procedures for the Safety Performance Evaluation of Highway Features*, 1993, National Cooperative Highway Research Program.

13. Hirsch, T.J., Administration, U.S.F.H., Institute, T.T., Highways, T.S.D.o. and Transportation, P., *Analytical Evaluation of Texas Bridge Rails to Contain Buses and Trucks*1978: The Institute.
14. Ghali, A., Neville, A.M. and Brown, T.G., *Structural Analysis: A Unified Classical and Matrix Approach*2003: Spon.
15. Alaywan, W.R., *Design, Behavior, and Performance of Precast Concrete Bridge Barriers*, Phd Dissertation 2011, *College of Engineering and Science*, Louisiana Tech University: Ruston, LA
16. Calloway, B.R., *Yield Line Analysis of an AASHTO New Jersey Concrete Parapet Wall*, M.S. Thesis 1993, *Civil Engineering*, Virginia Polytechnic Institute and State University: Blacksberg, VA
17. ASTM C 469-02, 2006e1, *Standard Method for Static Modulus of Elasticity and Poission's Ratio of Concrete in Compression*, ASTM International, West Conshohocken, PA, 2002, DOI:10.1520/C0469-02
18. ASTM E8 / E8M - 11, *Standard Test Methods for Tension Testing of Metallic Materials*, ASTM International, Conshohocken, PA, 2011, DOI:10.1520/0008_E0008M-11
19. ASTM C 618 - 08, *Standard Specification for Coal Fly Ash and Raw or Calcined Natural Pozzolan for Use in Concrete*, ASTM International, West Conshohocken, 2008, DOI:10.1520/C0618-12A